BIOCHEMISTRY
including biophysical chemistry & molecular biology

Article

pubs.acs.org/biochemistry

Probing Sequence-Specific DNA Flexibility in A-Tracts and Pyrimidine-Purine Steps by Nuclear Magnetic Resonance ^{13}C Relaxation and Molecular Dynamics Simulations

Evgenia N. Nikolova,[†] Gavin D. Bascom,[‡] Ioan Andricioaei,[‡] and Hashim M. Al-Hashimi*,[†]

[†]Department of Chemistry and Biophysics, University of Michigan, 930 North University Avenue, Ann Arbor, Michigan 48109, United States

[‡]Department of Chemistry, University of California, Irvine, California 92697, United States

Supporting Information

ABSTRACT: Sequence-specific DNA flexibility plays a key role in a variety of cellular interactions that are critical for gene packaging, expression, and regulation, yet few studies have experimentally explored the sequence dependence of DNA dynamics that occur on biologically relevant time scales. Here, we use nuclear magnetic resonance (NMR) carbon spin relaxation combined with molecular dynamics (MD) simulations to examine the picosecond to nanosecond dynamics in a variety of dinucleotide steps as well as in varying length homopolymeric $A_n{\cdot}T_n$ repeats (A_n-tracts, where n = 2, 4, or 6) that exhibit unusual structural and mechanical properties. We extend the NMR spin relaxation time scale sensitivity deeper into the nanosecond regime by using glycerol and a longer DNA duplex to slow overall tumbling. Our studies reveal a structurally unique A-tract core (for $n > 3$) that is uniformly rigid, flanked by junction steps that show increasing sugar flexibility with A-tract length. High sugar mobility is observed at pyrimidine residues at the A-tract junctions, which is encoded at the dinucleotide level (CA, TG, and CG steps) and increases with A-tract length. The MD simulations reproduce many of these trends, particularly the overall rigidity of A-tract base and sugar sites, and suggest that the sugar−backbone dynamics could involve transitions in sugar pucker and phosphate backbone BI ↔ BII equilibria. Our results reinforce an emerging view that sequence-specific DNA flexibility can be imprinted in dynamics occurring deep within the nanosecond time regime that is difficult to characterize experimentally at the atomic level. Such large-amplitude sequence-dependent backbone fluctuations might flag the genome for specific DNA recognition.

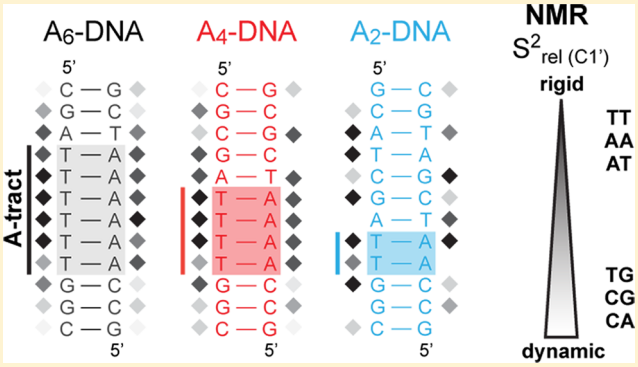

The DNA double helix is not simply a uniform structure that carries the codon message for gene expression. Rather, different nucleotide sequences show distinct propensities to deform, bend and twist, on their own[1,2] or upon binding to protein and drug targets.[3−5] Sequence-specific variations in DNA structure and flexibility form the basis of indirect DNA readout by regulatory proteins[6] and can also guide the positioning of nucleosomes along the genome.[7] These dynamic flags constitute a new layer of genetic information that remains poorly understood.

A crucial step toward decoding the functional roles of DNA sequence-specific mobility is to elucidate how the dynamic properties of duplex DNA vary with nucleotide sequence. Surveys of naked and protein-bound DNA crystal structures together with knowledge-based computational models have provided significant insight into the conformational flexibility of the DNA duplex at a dinucleotide level[3,8] and for longer nucleotide stretches.[9,10] These nearest-neighbor "rules" rank pyrimidine-purine (YR) steps, specifically CA, TG, TA, and CG steps, as the most conformationally flexible dinucleotide sequences. Not surprisingly, these steps are frequently the loci of helical deformations in DNA assemblies with transcription factors, and their flexibility features could guide indirect readout of specific DNA sequences.[11−13] On the other end of the spectrum, purine-purine (RR) AA steps, and less so purine-pyrimidine (RY) AT steps, are the most conformationally rigid dinucleotide steps and exhibit structural parameters that vary the least with sequence context, making them more difficult to mold by proteins.

Numerous studies reveal that poly(dA)·poly(dT) stretches, so-called asymmetric A_n-tracts ($n > 3$), adopt a locally distinct and rigid B-DNA conformation that forms cooperatively and cannot be purely described as a collection of individual AA steps as assumed by a nearest-neighbor model (reviewed by Haran[14]). This noncanonical conformation features a high propeller twist and negative inclination in A·T base pairs and a progressive narrowing of the minor groove in the 5′ to 3′

Received: July 16, 2012
Revised: September 28, 2012
Published: October 4, 2012

ACS Publications © 2012 American Chemical Society

dx.doi.org/10.1021/bi3009517 | *Biochemistry* 2012, 51, 8654−8664

direction.[15,16] The local conformational rigidity of A-tracts could explain their preferential exclusion from nucleosomes in vitro and avoidance in exon regions that are densely populated with nucleosomes in vivo.[17,18] Thus, A-tracts could be stereochemically locked into "inflexible" frameworks that could make them less prone to interact with outside regulatory factors. The local A-tract structure tends to resist sharp bending,[19] but A-tracts can induce macroscopic curvature when phased in tandem with the helical repeat,[20] which is enhanced by placement of CA/TG steps at their 5′ junction;[21] that is important for DNA looping in transcriptional regulation and chromatin packaging.[14] However, it remains unclear whether the local A-tract conformation or the helical bending is static or dynamic in nature or whether the global curvature of phased A-tracts originates at their junctions or is delocalized along the entire adenine stretch.[14] The ability of A-tracts to modulate DNA structure, and thus affect protein binding or allow long-range communication, has placed these unique elements at the forefront of research efforts to elucidate the relationship among structure, dynamics, and function in DNA transactions.

A growing number of experimental and computational studies show that sequence-specific DNA deformability observed in crystal structures is encoded as intrinsic dynamic fluctuations in naked DNA.[22−34] For instance, the discrimination of unwanted uracil, the product of cytosine deamination, from thymine by the uracil DNA glycosylase (UNG) repair enzyme that removes the modified base from genomic DNA was shown to be dictated by differences in thermally induced opening of A·U versus A·T base pairs.[35] More recently, Hoogsteen base pairs observed in duplex DNA bound to transcription factors[36,37] and antibiotic drugs[38] have been found to form spontaneously and sequence-specifically in naked duplex DNA.[33] Also, extruded nucleobases observed crystallographically within a junction between B-DNA and Z-DNA[39] have been shown to be sequence-specifically flexible in the context of B-DNA.[32] Moreover, experimental biophysical studies[31,40,41] and theoretical models[34] suggest that flexible CG steps, which are enriched in promoter regions and prone to C5-cytosine methylation as a mechanism for regulating gene expression, become more stiff and show a weaker propensity to circularize or form nucleosomes. Collectively, these studies suggest that the intrinsic dynamic properties of DNA can provide a mechanism for genetic control.

Nuclear magnetic resonance (NMR) spectroscopy is a powerful technique for studying DNA sequence-specific flexibility at atomic resolution and over time scales spanning picoseconds to seconds and longer. To date, NMR carbon spin relaxation studies targeting such specific biological sequences have uncovered large-amplitude backbone motions in cytosine sugars of unmodified DNA[22,27,28,42] and near sites of DNA damage[43] that may be important for specific DNA recognition. Surprisingly, no such NMR study has been used to explore sequence-specific flexibility of unusual A-tract sequences and systematically for dinucleotide steps and their dependence on immediate neighbors. Here, we use solution NMR spin relaxation techniques in conjunction with molecular dynamics (MD) simulations to probe the internal dynamics of varying length A-tracts. Our studies reveal a structurally unique A-tract with a uniformly rigid nucleotide core that exhibits a somewhat increased adenine over thymine sugar mobility. The A-tract is flanked by sequences that contain increasingly more flexible sugar moieties near the 5′ and 3′ A-tract junction steps with increasing A-tract length. We observe unique sugar mobility in pyrimidine residues, which seems to occur on nanosecond time scales based on measurements at variable temperatures and viscosities, that are encoded at the dinucleotide level but can be modulated by A-tract length. MD simulations reproduce the majority but not all of these trends and suggest that the sugar C1′ mobility could be coupled to rapid backbone transitions in BI ↔ BII and/or sugar pucker rearrangements.

MATERIALS AND METHODS

Materials and Sample Preparation. All unlabeled DNA oligonucleotides were purchased from Integrated DNA Technologies, Inc. (Coralville, IA). ^{13}C- and ^{15}N-labeled DNA dodecamers were synthesized in vitro by the method of Zimmer et al.[44] using a template hairpin DNA (IDT, Inc.), Klenow fragment DNA polymerase (NEB, Inc.), and uniformly ^{13}C- and ^{15}N-labeled dNTPs (Isotec, Sigma-Aldrich). Single-stranded DNA products were purified via 20% denaturing gel electrophoresis, isolated by passive elution from crushed gels, and desalted on a C18 reverse-phase column (Sep-pak, Waters). Oligonucleotides were further lyophilized, and complementary strands were resuspended separately in NMR buffer [15 mM sodium phosphate (pH 6.8), 25 mM sodium chloride, and 0.1 mM EDTA] supplied with 10% D_2O. Sample annealing was monitored by quick two-dimensional (2D) HSQCs until single-strand signals were no longer observed, with typically duplex concentrations of 0.5−1.0 mM for NMR studies. Unlabeled DNA constructs were prepared directly from oligonucleotides purchased from the manufacturer. Oligos were resuspended in NMR buffer at a concentration of ∼200 μM, and their concentration was measured by UV absorbance at 260 nm using extinction coefficients provided by the manufacturer. We annealed DNA duplexes by mixing an equal molar ratio of the complementary DNA strands, heating them for 2 min at 95 °C, and gradually cooling them at room temperature. DNA preparations were washed three times in resuspension buffer by microcentrifugation using an Amicon Ultra-4 centrifugal filter (3 kDa cutoff), concentrated to a volume of ∼250 μL (∼2−4 mM) for NMR studies and supplied with 10% D_2O.

NMR Measurements and Analysis. All NMR experiments were performed on a Bruker Avance 600 MHz NMR spectrometer equipped with a 5 mm triple-resonance cryogenic probe. Unlabeled DNA duplexes were assigned using conventional 2D ^{1}H−^{1}H NOESY (mixing time of 175 ms) in 10% D_2O at 26 °C. Proton assignments were transferred to 2D ^{1}H−^{13}C and ^{1}H−^{15}N HSQC spectra, allowing convenient assignment of base C2 H2, C6 H6, C8 H8, N1 H1, N3 H3, and sugar C1′ H1′ in unlabeled DNA constructs. Resonance intensities were obtained from ^{1}H−^{13}C and ^{1}H−^{15}N HSQC spectra and normalized for each type of bond vector to the intensity of a helical residue that was set to 0.1.

^{13}C relaxation rate constants R_1 and R_2 in ^{13}C- and ^{15}N-labeled DNA dodecamers were measured using a 2D $R_{1\rho}$ relaxation experiment[45] for base C2, C6, and C8 and sugar C1′ spins using a 3.5 kHz spin-lock field strength and a spin-lock carrier centered at C6 (for C2, C6, and C8) or C1′ resonances. Spin-lock powers were sufficiently high to suppress undesired chemical exchange contributions and ensure Hartmann−Hahn contributions of <1% for J_{CC} ∼ 10 Hz and <0.1% for J_{CC} ∼ 1 Hz. Relaxation data were collected with eight scans (∼6−7 h) and delay series for R_1 [20, 100, 250, and 450 (three times) ms] and $R_{1\rho}$ [4, 16, 32, and 48 (three times) ms] with triplicate measurements for error estimation. Relaxation

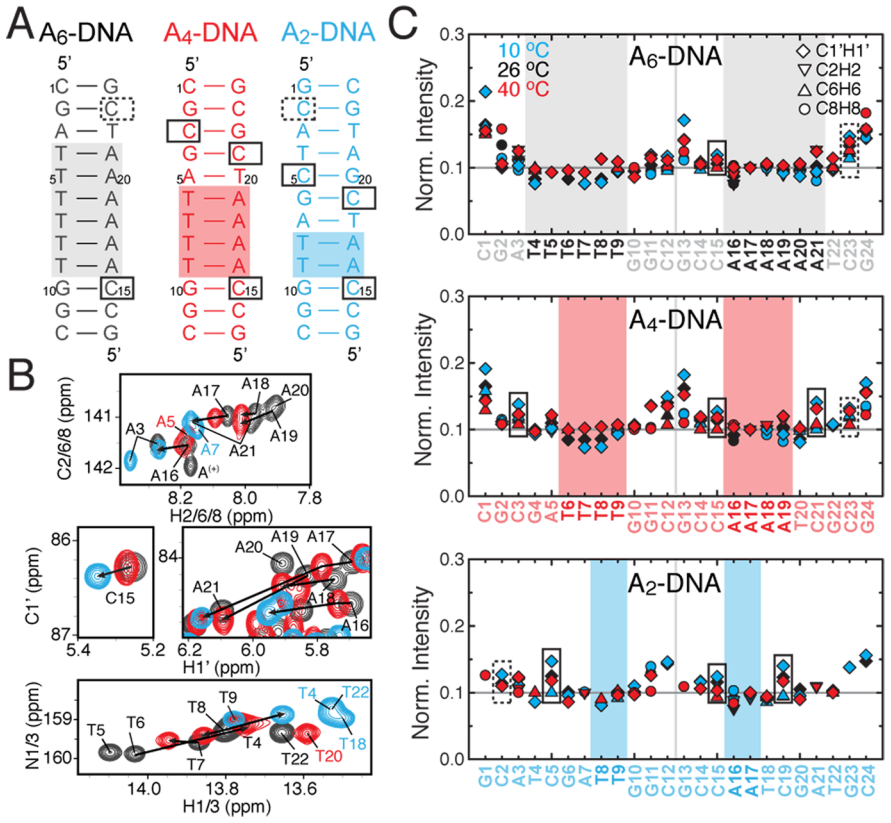

Figure 1. (A) DNA constructs for A_6-DNA (black), A_4-DNA (red), and A_2-DNA (blue). The A-tract position is highlighted, and flexible cytosines in CA/TG and CG steps are boxed, corresponding to plots in panel C. (B) NMR overlays of $^1H-^{13}C$ HSQC and $^1H-^{15}N$ HSQC spectra, color-coded for the three DNA sequences in panel A. (C) NMR resonance intensity profiles for base (C2 H2, C6 H6, and C8 H8) and deoxyribose (C1′ H1′) DNA sites obtained from 2D $^1H-^{13}C$ HSQC spectra at three temperatures (see the inset). Boxed residues correspond to cytosine sugar sites that show enhanced intensities and also an unusual increase in intensity with lower temperatures (near terminal sites are dashed).

profiles were processed with nmrPipe[46] and relaxation rate constants determined by fitting the resonance intensities to monoexponential decays using Mathematica 6.0 (Wolfram Research, Inc.). R_2 relaxation rates were computed from R_1 and $R_{1\rho}$ using the relationship $R_2 = (R_{1\rho} - R_1 \cos^2 \theta)/\sin^2 \theta$.[47] Relative order parameters (S_{rel}^2) were computed as $2R_2 - R_1$ values normalized to the largest value from a helical region for each carbon type (C2, C6, C8, or C1′), and also each residue type for C8 and C6, set to unity.[45,48,49] Hydrodynamic and S^2 predictions were conducted with HydroNMR[50] and in-house software by employing a previously described protocol[45] with a DNA model constructed with 3DNA[51] or obtained from MD simulations, assuming anisotropic diffusion and using only R_1 and R_2 values (without heteronuclear NOEs).

Molecular Dynamics Simulations. Atomic coordinates were built using the Nucleic Acid Builder (part of AmberTools[52]) of sequence (A_2-, A_4-, and A_6-DNA) in ideal helical B-form DNA. The structures were solvated with water and Na^+ ions using Visual Molecular Dynamics[53] in a 64 Å × 64 Å × 64 Å cube, with 25 Na^+ ions and three Cl^- ions to neutralize charge and bring molarity to the experimental conditions. All structures were heated gradually with harmonic constraints placed on sugar−phosphate backbone atoms from 0 to 300 K in 150000 steps, with 1 fs time steps in NAMD using a Langevin thermostat[54] with the CHARMM force field.[55,56] Harmonic constraints were gradually released over 300 ps, and the systems were equilibrated for 10 ns each. Independent trajectory ensembles were then generated from 10 independent Maxwell−Boltzmann distributed initial conditions for each sequence, producing 30 uncorrelated trajectories of 10 ns each.

S^2 values were determined using a generalized Lipari−Szabo model free approach[57,58] in which the bond−bond autocorrelation function for the second-order Legendre polynomial describing rotational decorrelation is parametrized by the sum of two-exponential forms[59] to yield the amplitude (S^2) and correlation time (τ) according to the following relationship:

$$C(t) = S^2 + (1 - S_f^2)e^{-t/\tau_f} + (S_f^2 - S^2)e^{-t/\tau_s}$$

where $S^2 = S_f^2 S_s^2$ is the plateau of the function and subscripts f and s refer to fast and slow motions, respectively, which are thought to be uncorrelated. As a check of convergence, S^2 values were also calculated from the bond vector Cartesian coordinate equilibrium expression given by Szabo and Henry,[60] which gave good agreement with the extended exponential fit. Overall tumbling was removed by least-squares fit alignment of heavy atoms in VMD.[53] Time correlation functions were calculated using the CHARMM software package.[58,61] Plateau values at 1 ns (i.e., one-tenth of the total trajectory time[62]) were determined by averaging the tail autocorrelation function values, and the results were then averaged across ensembles. Sugar pucker statistics and sugar−backbone dihedral angles were calculated from the MD trajectories using 3DNA.[51]

RESULTS

A-Tract-Specific Dynamics from NMR Spectra and Resonance Intensities. We used solution NMR to study the

dx.doi.org/10.1021/bi3009517 | Biochemistry 2012, 51, 8654−8664

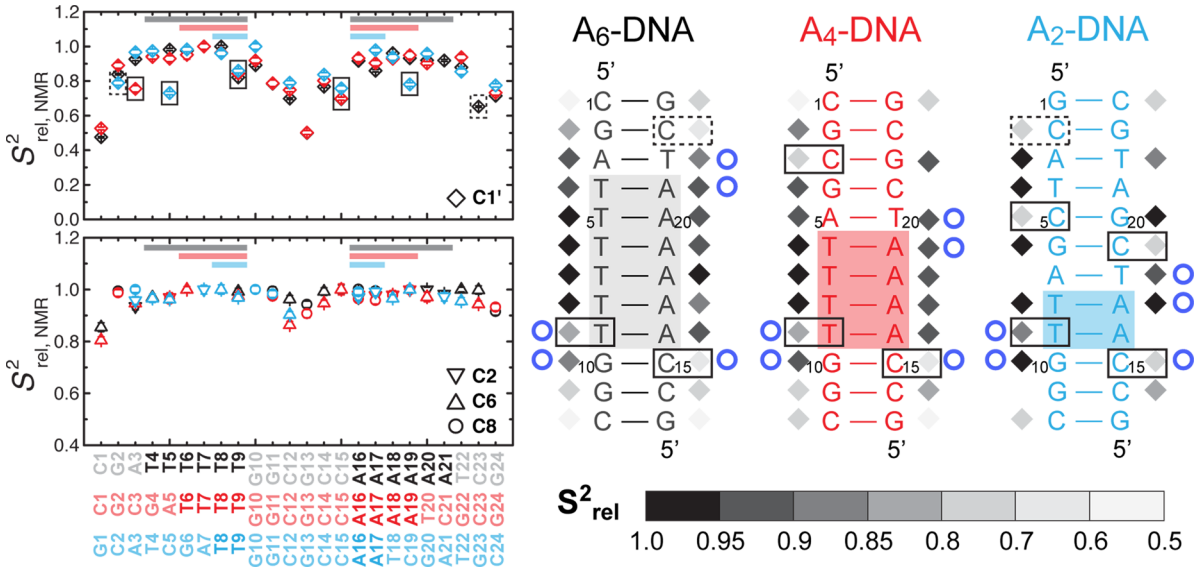

Figure 2. Relative order parameter S_{rel}^2 (left) obtained from ^{13}C NMR spin relaxation data for base (C2 H2, C6 H6, and C8 H8) and deoxyribose (C1′ H1′) sites in A_6-DNA, A_4-DNA, and A_2-DNA (26 °C) and DNA constructs (right) showing the variation in sugar backbone S_{rel}^2 (diamond). Pyrimidine residues with reduced sugar C1′ S_{rel}^2 values are boxed in plots and DNA sequences (near terminal sites are dashed), while A-tract junction residues that are modulated by A-tract length are marked with a blue circle.

dynamic properties of three uniformly ^{13}C- and ^{15}N-labeled DNA dodecamers containing two (A_2-DNA), four (A_4-DNA), and six (A_6-DNA) adjacent adenines capped by GC-rich helices (Figure 1A). A_6-DNA appears in a context (5′ CA_6T) commonly encountered in kinetoplast DNA, which was originally found to exhibit microscopic bending when regularly phased with the helical repeat (~10.5 bp/turn).[63]

We first examined the NMR spectral variations as a function of A-tract length. $^1H-^{13}C$ HSQC and 2D NOESY spectra of A_6-DNA and A_4-DNA displayed chemical shifts (CSs) and nuclear Overhauser effect (NOE) connectivities characteristic of asymmetric A-tracts,[64,65] which have been shown to deviate from a canonical B-DNA conformation.[15] For example, we observed strong interstrand NOE cross-peaks between the nucleobase H2 proton of adenine and the sugar H1′ or imino H3 protons of the 3′-neighboring thymine on the complementary strand (data not shown), which has previously been correlated with minor groove compression and a large propeller twist.[64,65] In addition, purine H8/H1′ and pyrimidine H3/H1′ protons typically displayed upfield- and downfield-shifted CSs, respectively, characteristic of A-tract sequences (Figure 1B). The highly unusual upfield shifted proton CS of the cytosine and adenine sugar moiety at the 5′ CA/TG junction also represents a unique spectral signature of the distinct A-tract conformation.[64,65]

The NMR spectroscopic signatures of the A-tract described above diminish slightly in magnitude from A_6-DNA to A_4-DNA and are no longer observed in A_2-DNA that does not adopt the unusual conformation of longer adenine runs or induce any appreciable global curvature when periodically phased relative to a random sequence (Figure 1B). Specifically, curtailing the A-tract from six to two AT base pairs caused a downfield shift for adenine H8/H1′ and an upfield shift for thymine H3/H1′ protons, in the direction of the CS space generally occupied by heterogeneous sequences (Figure 1B). Certain base and sugar protons at the common 5′ CA/TG junction (C15 H1′ and A16 H8/H1′) also experienced significant downfield shifts from A_6-DNA to A_4-DNA (up to 0.04 ppm) and once again an even larger shift (up to 0.2 ppm) from A_4-DNA to A_2-DNA. Such sizable perturbations in proton CSs are not expected to arise because of remote changes in sequence (>2 bp away) and point to conformational changes within the A-tract that vary with A-tract length.

We further investigated the dynamic behavior of DNA dodecamers by comparing spin-normalized resonance intensities for nucleobase C2 H2, C6 H6, and C8 H8 and deoxyribose C1′ H1′ spin pairs (Figure 2C). The resonance intensity provides a qualitative assessment regarding the relative mobility for a given site over time scales spanning picoseconds to milliseconds and/or variations in bond vector orientation relative to the magnetic field.[45,66,67] Generally, high peak intensity or line narrowing is associated with increased net dynamics (local or collective) at a given site on the pico- to nanosecond time scale, whereas weak peak intensities could reflect relative rigidity on the pico- to nanosecond time scale, micro- to millisecond conformational exchange, and/or an orientation for the bond vector that is more parallel with respect to the long duplex axis.

As expected, we observed increased intensities for residues near the terminal end likely arising from end fraying at pico- to nanosecond time scales. Although, in general, the intensities observed within the duplex are quite uniform, some unique dynamic signatures are apparent. We observed reduced intensities at the 5′ CA/TG A-tract junction (C8 H8 and C2 H2 of A16), which points to micro- to millisecond chemical exchange that we previously showed corresponds to transient excursions toward noncanonical Hoogsteen base pairs.[33] In addition, we observe elevated intensities for cytosine and thymine sugar C1′ H1′ sites in CA and CG steps that indicate elevated pico- to nanosecond sugar flexibility similar to those previously observed for cytosines in CG steps embedded inside a different DNA sequence.[28] Interestingly, these normalized intensities increase when the temperature is reduced from 40 to 10 °C (Figure 2C). This suggests the presence of sugar–backbone fluctuations occurring on nanosecond time scales that are masked by overall rotational diffusion; lowering the

dx.doi.org/10.1021/bi3009517 | Biochemistry 2012, 51, 8654–8664

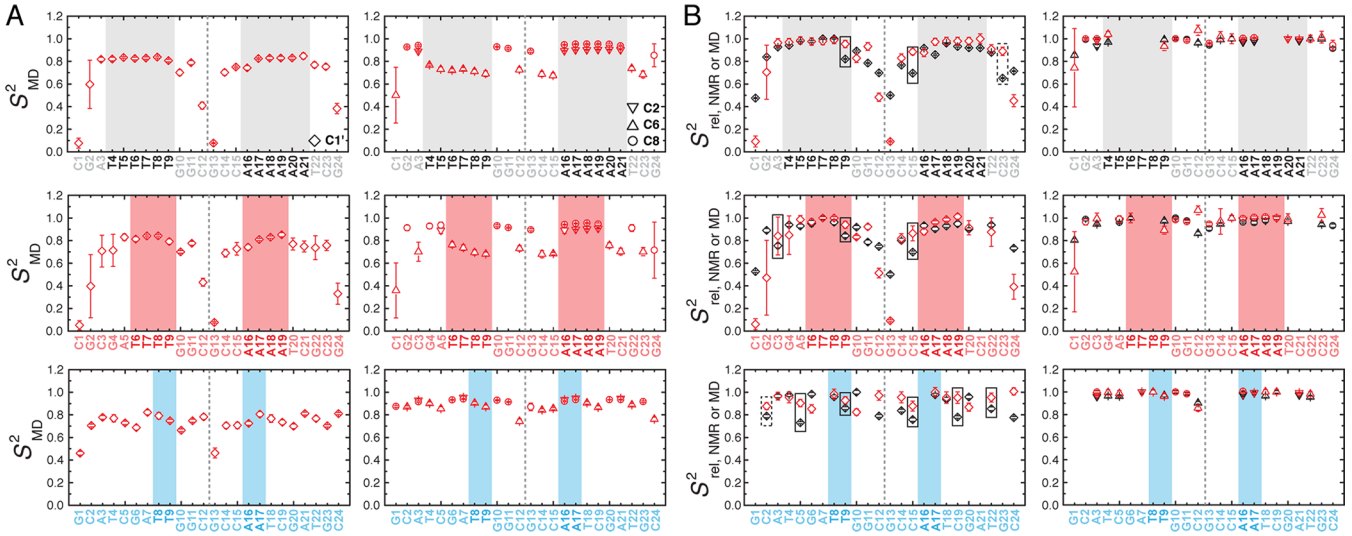

Figure 3. (A) S^2 order parameters obtained by MD simulations for base (C2 H2, C6 H6, and C8 H8) and deoxyribose (C1′H1′) sites in A_6-DNA, A_4-DNA, and A_2-DNA. (B) Comparison between relative order parameter S_{rel}^2 obtained by NMR ^{13}C spin relaxation and MD simulations. Pyrimidine residues with reduced sugar C1′ S_{rel}^2 values are boxed (near terminal sites are dashed).

temperature decouples the two motions by slowing overall diffusion, allowing better resolution of the local dynamics.[66,67]

Picosecond to Nanosecond Dynamics from Carbon Spin Relaxation Measurements. We used carbon ^{13}C spin relaxation measurements[68,69] to more quantitatively characterize pico- to nanosecond dynamics in the three DNA constructs. Specifically, we measured longitudinal (R_1) and transverse (R_2) ^{13}C spin relaxation data for C2, C6, C8, and C1′. The measured R_1 and R_2 values were then used to compute a relative order parameter, S_{rel}^2,[49,57] which provides an estimate for relative motional amplitudes across different sites (Figure 2B). The value of S_{rel}^2 ranges from zero for a highly flexible site to one for a perfectly rigid site. The values were normalized independently for each carbon type relative to the most rigid site.[49]

The S_{rel}^2 values reinforced many of the trends obtained from analysis of the resonance intensities (Figure 2). The nucleobases of nonterminal residues were uniformly rigid across different residues and DNA constructs (S_{rel}^2 range of ~0.94−1.0) (Figure 2). The sugar moieties exhibited larger variations in S_{rel}^2 values that cannot be ascribed to typical variations in C1′ H1′ bond vector orientation (Figure 2). Within the A-tract, thymine C1′ sites exhibited the lowest flexibility with fairly uniform S_{rel}^2 values approaching unity. Somewhat higher sugar flexibility was observed at the complementary adenine residues in the longer A-tracts of A_6-DNA and A_4-DNA (average S_{rel}^2 ~ 0.92) (Figure 2). The highest flexibility was seen for the second adenine from the 5′ junction in A_6-DNA (A17) that gradually diminished with shortening of the A-tract (S_{rel}^2 from 0.86 to 0.98). Similar A-tract-dependent sugar−backbone dynamics were observed for residues at the A-tract junctions, including the common G10 and T9 at the 5′ junction and the variable adenine (A17, A19, and A21) and thymine (T18, T20, and T22) at the 3′ junction (Figure 2). Overall, the pattern of enhanced sugar−backbone dynamics at the junctions with longer A-tracts correlated well with the conformational changes observed by NMR chemical shift and NOE data, which indicates that the increased local mobility arises in part from a shift toward a distinct conformation. Once again, we observed elevated sugar−backbone pyrimidine dynamics in YR dinucleotide steps, specifically for CA/TG (T9 and C15 in all DNAs; C2 and T22 in A_2-DNA) and CG (C3 in A_4-DNA; C5 and C19 in A_2-DNA) steps with greater mobility observed in cytosine (S_{rel}^2 ~ 0.65−0.78) than in thymine (S_{rel}^2 ~ 0.82−0.86) sugars. These motions were less dependent on A-tract length when the YR step was placed at the 5′ A-tract junction. Thus, it follows that the pico- to nanosecond motions at YR sites that are known to be flexible are encoded at the sequence-specific dinucleotide level rather than their position relative to or length of the A-tract.

Dynamics of A-Tract and Dinucleotide Sequences from MD Simulations. Next, we conducted an analysis of the set of ten 10 ns molecular dynamics (MD) simulations for each of the sequences to gain further insights into the dynamics observed using NMR relaxation. We first compared results from the MD simulations with the NMR data by computing generalized order parameters (S^2) from the autocorrelation function averaged over ten simulation runs (Figure 3A). These order parameters were converted into S_{rel}^2 values using an approach analogous to the NMR relaxation analysis (Figure 3B). Below, we focus on trends rather than quantitative comparison of S_{rel}^2 values given the relatively short MD simulations and the fact that the determination of S_{rel}^2 rather than absolute S^2 values complicates quantitative comparisons.

In agreement with NMR data, uniform and high S_{rel}^2 values were observed for nonterminal nucleobase sites, independent of A-tract length (Figure 3B). Likewise, overall lower S_{rel}^2 values and greater disorder were observed for terminal nucleobase and particularly sugar C1′ sites that are consistent with end fraying effects (Figure 3B). More importantly, the simulations captured the decreased and uniform mobility for the thymine and most adenine sugars within the A-tract core and the tendency for increased sugar mobility at the junction residues of longer A-tracts compared to that of the central residues. Similar to NMR observations, cytosine and thymine sugars in YR steps displayed lower S_{rel}^2 values than pyrimidines in central A-tract positions, although their flexibility was underestimated by MD versus NMR.

At the same time, many of the specific trends observed by NMR were not very well reproduced by the MD simulations.

dx.doi.org/10.1021/bi3009517 | *Biochemistry* 2012, 51, 8654−8664

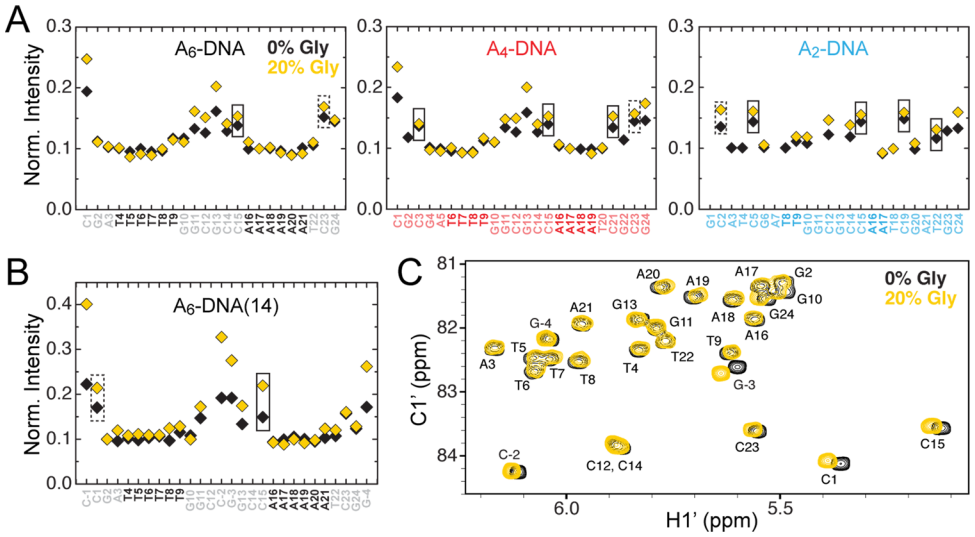

Figure 4. (A) NMR resonance intensity profiles for base (C2 H2, C6 H6, and C8 H8) and deoxyribose (C1′ H1′) sites in A_6-DNA, A_4-DNA, and A_2-DNA obtained in the absence (black) and presence (yellow) of 20% glycerol. Pyrimidine residues with reduced sugar C1′ S_{rel}^2 values that show increases in intensity with addition of glycerol are boxed in the plots (near terminal sites are dashed). (B) Corresponding intensity profiles for A_6-DNA(14). (C) Overlay of 2D $^1H-^{13}C$ HSQC spectra of A_6-DNA(14) in the absence and presence of 20% glycerol.

Notably, the increasing sugar C1′ flexibility with A-tract length at the shared 5′ G10 and T9 residues was not observed in the MD data. Instead, MD C1′ S_{rel}^2 values for these sites exhibited little to no variation with A-tract length, with the thymine being more rigid and the guanine being more flexible than they were when they were measured by NMR. More generally, internal C1′ spins exhibited greater dynamic variability in MD simulations as the nucleotide sequence became more heterogeneous from A_6-DNA to A_2-DNA, especially because of the increases in guanine sugar dynamics in A_2-DNA that were not observed by experiment. These discrepancies may be due to insufficient sampling within the simulation time frame or uncertainties in the structures used to conduct the simulations or may represent deficiencies in the force field. The MD simulations also show behavior that is not observed by NMR, including the observation of elevated levels of motion in C6 sites for A_6-DNA and A_4-DNA but not for A_2-DNA (Figure 3A). These motions are not expected on the basis of previous NMR–MD studies[27,28] and model-free S^2 calculations performed here (data not shown).[45] Therefore, these differences likely do not represent true differences in dynamics between C8 H8 and C6 H6 bond vectors but, rather, signify an issue with nucleobase force field parametrization that may stem from more homogeneous sequences (i.e., A-tracts) not being used in initial parameter optimization.

Not withstanding some of the discrepancies between NMR and MD, good agreement was obtained for the general trends of intrinsic DNA mobility within A-tracts, some junction sites, and flexible pyrimidine residues in YR steps. Therefore, we examined the MD trajectories more closely to gain insight into the molecular motions that underlie the observed variations in sugar and base S_{rel}^2. Analysis of sugar pucker distributions and time-dependent fluctuations revealed that purines, especially in A-tracts, adopted primarily South (S, C2′-*endo*/C3′-*exo*) sugar pucker angles with rare and short-lived transitions toward North (N, C3′-*endo*/C2′-*exo*) conformers, while pyrimidines exhibited greater diversity in sugar pucker angles with more frequent and long-lived transitions to noncanonical North and East (E, O4′-*endo*) conformers (Figure S1 and S2 of the Supporting Information). For example, T9 at the 5′ A-tract junction and in a TG step occupied the C3′-*endo* state at least 20% of the time, which gradually increased to ∼50% with longer A-tracts. Core A-tract thymines also exhibited larger C3′-*endo* populations relative to those of their adenine partners. Interestingly, the broadest sugar pucker distribution with a significant fraction of E states (∼30%) was adopted by thymines in AT steps and was independent of A-tract length. Thus, the greater population of noncanonical C3′-*endo* puckers that entail large-amplitude sugar motions (∼150°) observed for thymine and cytosine residues by MD could partially account for the reduced sugar C1′ order parameters observed at YR steps by NMR. The higher proportion of C3′-*endo* sugar puckers in A-tract thymines and especially in cytosines is also reflected in their more downfield-shifted C1′ chemical shifts versus those for purines.[33] However, the appreciable C3′-*endo* populations in central A-tract thymines versus adenines could not explain the lower pyrimidine sugar mobility there. Sugar repuckering events were always accompanied by much lower amplitude (<50°) changes in the glycosidic torsion angle χ toward a high *anti* base orientation, which can also explain the absence of increased mobility in DNA bases for nonterminal sites of increased sugar mobility (Figure S2 of the Supporting Information).

We further examined the equilibrium between BI ↔ BII backbone phosphate conformers that could potentially give rise to high-amplitude sugar–backbone motions. The major BI and minor BII backbone phosphate states are determined by the difference in ε and ζ dihedral angles ($\varepsilon - \zeta < 0$ for BI, and $\varepsilon - \zeta > 0$ for BII). The BII conformer occurred most frequently in terminal nucleotides (15–65%), followed by CG, CA, and TG steps (∼4–20%) and, finally, adenines within A-tracts (3–5%) (Figure S3 of the Supporting Information). The BII conformer was nearly absent in the backbone of internal A-tract thymines. This trend in BII populations resembles closely the trend in NMR C1′ S_{rel}^2 values and could be used to explain the gradation in sugar mobility across different dinucleotide steps and A-tract motifs in DNA duplexes. Together, analysis of the MD DNA simulations suggested that deoxyribose order

dx.doi.org/10.1021/bi3009517 | *Biochemistry* 2012, 51, 8654–8664

parameters obtained by NMR relaxation could be influenced by both backbone BI ↔ BII and sugar pucker transitions, which is consistent with a previously established correlation among ensemble BII, S sugar populations, and C1′ order parameters obtained solely by NMR.[23] However, we did not observe direct coupling between the BI ↔ BII and sugar S ↔ N repuckering fluctuations, suggesting that these two motions could be semi-independent of each other.

Probing Nanosecond Motions by Slowing Overall Tumbling. Apart from uncovering an overall helical rigidity in A-tracts of four to six consecutive adenines, we found large-amplitude fluctuations of pyrimidine sugar C1′ H1′ bond vectors in two types of YR dinucleotide steps, CA, TG, and CG steps. On the basis of the temperature dependence of resonance profiles, it appeared that these motions occurred on relatively slower time scales, possibly within the nanosecond window. To probe whether the elevated flexibility at YR steps represents nanosecond motions, we devised a strategy to selectively slow global molecular diffusion and reduce the level of coupling between internal and overall dynamics that would resolve such motions. Our goal was to achieve these conditions without the use of multiple isotopically labeled samples that are required by a domain elongation approach.[66] We employed a combination of minimal elongation of unlabeled DNA samples and glycerol addition, which increases the solvent (water) viscosity and retards the overall rotational diffusion in a predictable manner. Specifically, we collected resonance intensities for unlabeled DNA constructs of the same size (12-mer) or elongated by one C·G base pair on each end (14-mer) in the absence and presence of 20% (v/v) glycerol.

First, as a benchmark for this method, we used a 27-nucleotide HIV-1 TAR construct containing a mutant UUCG tetraloop (mTAR), whose nanosecond dynamics have been extensively characterized by ^{15}N[66] and ^{13}C[45] spin relaxation using a helical elongation technique. Upon addition of ∼25% (v/v) glycerol that increases the rotational correlation time of mTAR from ∼6 to ∼11 ns, we observed line narrowing for several nucleotides that were among those previously shown to exhibit nanosecond internal dynamics (data not shown).[66]

To probe for nanosecond motions in DNA sugars, implied by the reduced S_{rel}^2 parameters, resonance intensities were first measured for C1′ H1′ of unlabeled A_6-DNA, A_4-DNA, and A_2-DNA in the presence ∼20% glycerol that is expected to increase the duplex rotational correlation time (τ_m) by ∼1.6 times to ∼7.2 ns at 26 °C (Figure 4). The intensity profiles showed a selective increase in peak intensity at cytosines that were part of CA and CG steps as well as terminal residues (Figure 4A). This suggested that the increased backbone dynamics could involve slower, nanosecond motions that are absent or suppressed in other sequence contexts. The effect was even more pronounced when the same experiment was repeated with a 14-mer A_6-DNA [A_6-DNA(14)], for which we obtained an up to 1.5 times larger fractional increase in intensities as compared to those of 12-mer A_6-DNA (Figure 4B). There, the longer DNA with respectively slower diffusion (τ_m ∼ 9 ns in 20% glycerol) allowed us to probe even deeper into the nanosecond window. Moreover, a noticeable increase in C1′ H1′ intensity was observed for the AT step at the 3′ A_6-tract junction that hinted toward nanosecond dynamics at that site as well. The nearly perfect spectral overlay with and without the retarding agent excluded the possibility that changes in the duplex dynamics are a result of specific interactions with glycerol or major structural changes in DNA (Figure 4C).

DISCUSSION

In this study, we examine the conformation and dynamics of DNA sequences that contain variable length A-tracts using experimental solution NMR carbon relaxation in conjunction with computational simulations. Our data indicate variations in DNA flexibility that are dependent on A-tract length as well as local dinucleotide environment and support the presence of sequence-specific DNA dynamics. Moreover, such differences in the internal pico- to nanosecond dynamics are found to reside primarily at the DNA sugar backbone, which can be easily accessed by DNA-targeting agents and utilized by proteins and small molecules for indirect readout of specific DNA sequences, nucleotide modifications, and damaged sites.

First, the chemical shift analysis confirmed the unusual structure adopted by longer A-tracts and provided evidence of A-tract length-dependent conformational changes near the 5′ and 3′ junctions. These changes correlated with the increase in internal backbone dynamics for residues near the A-tract junctions as the A-tract was elongated. This implies that heterogeneity in DNA dynamics of different sequences may correlate with sequence-specific DNA structure. Analysis of the resonance intensities and ^{13}C spin relaxation profiles indicated that the sugar moiety, but not the base, of residues found at A-tract junctions progressively gained flexibility with longer A-tracts, while base and sugar sites of core A-tract residues, especially thymines, remained rigid. Order parameters obtained from MD simulations of the DNA dodecamers yielded excellent agreement with trends of internal mobility for core and certain junction A-tract residues. Some discrepancies in S_{rel}^2 values could be rationalized by inadequate sampling in the MD runs or inaccurate duplex structures. Thus, it seems that as the A-tract becomes longer and stiffer (up to a certain point) by stacking AA steps that collectively favor a distinct B-DNA conformation, residues at the A-tract ends become increasingly flexible and perhaps subject to helical deformations to retain a favorable base stacking arrangement with the A-tract. We cannot rule out large-scale helical bending motions as the source of the enhanced backbone dynamics at A-tract junctions, even though such motions could not be previously detected using a DNA domain elongation approach.[67]

The structural rigidity of A-tracts is not a new concept. As discussed before, AA steps comprising longer A-tracts are ranked as the most rigid dinucleotide sequences. Moreover, increased base pair stability[70] and helical stiffness[19] have been observed for poly(dA)-poly(dT) sequences of at least three consecutive A·T base pairs. However, here we report the first quantitative NMR relaxation study of pico- to nanosecond dynamics confirming that A-tract residues do not exhibit unusual large-amplitude base or sugar motions, except for residues near the junctions. The formation of these inflexible DNA blocks of AA steps can be traced to their strong conformational preference to adopt a large propeller twist and limited slide mobility that could have a severe stereochemical locking effect and, in principle, introduce mechanical strain into longer A-tracts, yet its effect could be potentially offset by stabilizing interactions (improved $\pi-\pi$ base stacking, bifurcated hydrogen bonds, and formation of an ordered hydration spine in the narrow minor groove, coupled with helical bending) that are proposed to be specific features of A-tract sequences based on a number of biochemical and biophysical studies[14] but that

dx.doi.org/10.1021/bi3009517 | Biochemistry 2012, 51, 8654−8664

still remain controversial. The distinct structure and higher rigidity of A-tract motifs, granted by these interactions, could stabilize helical bends or a narrow minor groove, which frequently serves as an accessory indirect recognition site in the transcription factor binding to its cognate DNA.[12]

The NMR data also revealed extensive sugar, but not base, dynamics at C1′ spins of cytosine and thymine nucleotides located in CA, TG, and CG sequences that appear to be a general feature of pyrimidine-purine dinucleotide steps. The intensity data at different temperatures and glycerol levels strongly suggest that these dynamics, particularly in cytosine nucleotides, occur on nanosecond time scales and are suppressed in purine nucleotides. The ^{13}C relaxation data further showed that these dynamics are somewhat modulated by the A-tract size when the step was positioned at the 5′ A-tract junction and by variable nearest-neighbor nucleotides (i.e., TCG vs GCG). Moreover, the trend of reduced order parameters at these sites, but not the extent of these amplitudes, was captured by MD simulations; this likely results from undersampling (i.e., from broken ergodicity) and/or structural discrepancies between NMR and MD ensembles. These differences can be addressed in the future by running longer MD simulations and possibly by using known NMR structures as initial DNA coordinates.

Previously, several solution NMR investigations have reported increased backbone disorder in cytosine and, less so, in thymine sugars of the YR (CG, CA, TG, and TA) and YY (CT or TC) context in B-DNA.[22,27,28,43] While the anomalously high mobility of cytosine sugars was linked to cytosine-specific backbone motions and the sequence dependence was understressed, the higher mobility of thymine sugars at TG (and TA) steps relative to more rigid TT and AT steps has escaped attention likely because of the paucity of sequence-specific probes. Also, there is previous evidence of nanosecond motions at CG dinucleotides,[41] which we extend here to the CA dinucleotide. There, the observation of increased flexibility at the *Hha*I methyltransferase target dodecamer comprised of two CG steps by both solid and solution state NMR, which are sensitive to different time scales, could be reconciled with a specific motional model that involves slower-than-diffusion cytosine sugar fluctuations.[41]

Indeed, the events that underlie these molecular transitions are difficult to probe solely by NMR. The development of motional models for DNA flexibility can benefit tremendously from state-of-the-art computational simulations, as has been demonstrated for canonical,[28,33] noncanonical,[71] and damaged[72] DNA. In one particular NMR study informed by MD, Duchardt et al. proposed a motional model for the rapid picosecond mobility observed at cytosine sugar moieties that involves sugar repuckering (S ↔ N) transitions.[28] This model, supported by the stronger preference of cytosines for the N conformer determined by experiment and ab initio calculations,[73,74] could well be physically plausible. Here, analysis of the sugar pucker distributions and repuckering transition rates in MD simulations with DNA sequence also uncovered increased populations and longer lifetimes for noncanonical N (C3′-*endo*) conformers in cytosines and thymines located in CA, TG, and CG steps as compared to other sequences. The increased population of N puckers in A-tract thymine and especially cytosine sugars is further supported by the more downfield-shifted C1′ chemical shifts. At the same time, we found that the backbone for pyrimidines in CG, and less so in CA and TG, steps was particularly enriched with the minor BII conformer. These findings are in agreement with prior solution NMR studies based on ^{31}P chemical shifts, $^{3}J_{H3'\text{-}P}$ couplings, and interproton distances as well as with surveys of DNA crystal structures and MD simulations showing that the BI ↔ BII balance is sequence-specific, with the rare BII conformation having a higher occupancy in CA, TG, and CG dinucleotide steps.[75−77] These two sugar−backbone motions, which do not appear to be directly coupled to each other from the MD trajectories, could provide a plausible explanation for the markedly lower C1′ order parameters at YR steps.

The increased populations of C3′-*endo* states within core A-tract thymines over adenines in MD failed to explain the somewhat higher thymine C1′ order parameters obtained by experiment. However, we observed a direct link between the lower mobility of A-tract thymines and negligible fractions of the minor BII conformer, which were at least 10-fold higher in the opposite adenines or in TG steps. Therefore, we hypothesize that excursions to the minor BII conformer could in fact contribute to the C1′ order parameters for internal nucleotides. In conjunction with this hypothesis is a study that links stabilization of the BI over BII backbone conformer of cytosines upon C5 methylation observed by MD[78] with dampened sugar and phosphate backbone dynamics observed by NMR.[31,40,41] These findings give credence to the emerging idea that MD simulations are capable of providing physically relevant models for the intrinsic dynamics of nucleic acids and their sequence dependence.

In a biological context, unusual sugar−backbone dynamics can ultimately facilitate recognition of specific DNA sequences by their protein or small molecule binders. NMR−MD studies by the groups of Schleucher[28] and Drobny and Varani[27,40,41] have made significant progress in understanding the sugar−backbone dynamics of AT-rich *Eco*RI endonuclease and CG-rich *Hha*I methyltransferase target sites as well as the impact of methylation at CG steps on backbone flexibility, which may play a role in methylation-dependent protein recognition. Flexible CA/TG steps are also targeted by many biological factors, such as the ubiquitous and gene-regulating CAP[12,79] and p53[80] proteins that are known to induce large deformations or trap noncanonical base pairing conformations. Similar recognition strategies that take advantage of sequence-specific duplex flexibility are also utilized by DNA-binding drugs.[5] DNA is emerging as a prominent drug target, and effective tools for analysis of DNA−drug recognition can facilitate the development of therapeutics. Thus, the prospect of engineering gene regulation by protein− or drug−DNA interactions places tremendous importance on how well we understand and can manipulate sequence-dependent DNA dynamics.

■ ASSOCIATED CONTENT

Supporting Information

NMR spin relaxation data and sugar pucker and dihedral angle statistics derived from the MD simulations. This material is available free of charge via the Internet at http://pubs.acs.org.

■ AUTHOR INFORMATION

Corresponding Author

*Department of Chemistry and Biophysics, University of Michigan, 930 N. University Ave., Ann Arbor, MI 48109-1055. Phone: (734) 615-3361. Fax: (734) 647-4865. E-mail: hashimi@umich.edu.

Author Contributions

E.N.N. performed and analyzed the NMR experiments. G.D.B. performed and analyzed the MD simulations with the help of E.N.N. and I.A. E.N.N. and H.M.A.-H. wrote the manuscript with input from G.D.B. and I.A.

Funding

This work was supported by National Institutes of Health Grant R01GM089846 to H.M.A.-H. and I.A. E.N.N. acknowledges support by a Rackham International and Predoctoral Fellowship awarded by the University of Michigan.

Notes

The authors declare no competing financial interest.

■ ACKNOWLEDGMENTS

We thank Dr. Alexandar L. Hansen for help with NMR experimental setup and Dr. Alexander V. Kurochkin for NMR expertise and maintenance. We gratefully acknowledge the Michigan Economic Development Corp. and the Michigan Technology Tri-Corridor for support in the purchase of a 600 MHz spectrometer. Calculations were performed on the supercomputing cluster Greenplanet at the University of California, Irvine, made possible by National Science Foundation Grant CHE-0840513.

■ ABBREVIATIONS

NMR, nuclear magnetic resonance; MD, molecular dynamics; A, adenine; G, guanine; C, cytosine; T, thymine; Y, pyrimidine; R, purine; UNG, uracil DNA glycosylase; HSQC, heteronuclear single-quantum correlation; NOESY, nuclear Overhauser effect spectroscopy.

■ REFERENCES

(1) Yanagi, K., Prive, G. G., and Dickerson, R. E. (1991) Analysis of local helix geometry in three B-DNA decamers and eight dodecamers. *J. Mol. Biol. 217*, 201−214.

(2) Dickerson, R. E. (1998) DNA bending: The prevalence of kinkiness and the virtues of normality. *Nucleic Acids Res. 26*, 1906−1926.

(3) Olson, W. K., Gorin, A. A., Lu, X. J., Hock, L. M., and Zhurkin, V. B. (1998) DNA sequence-dependent deformability deduced from protein-DNA crystal complexes. *Proc. Natl. Acad. Sci. U.S.A. 95*, 11163−11168.

(4) Svozil, D., Kalina, J., Omelka, M., and Schneider, B. (2008) DNA conformations and their sequence preferences. *Nucleic Acids Res. 36*, 3690−3706.

(5) Arauzo-Bravo, M. J., and Sarai, A. (2008) Indirect readout in drug-DNA recognition: Role of sequence-dependent DNA conformation. *Nucleic Acids Res. 36*, 376−386.

(6) Rohs, R., West, S. M., Sosinsky, A., Liu, P., Mann, R. S., and Honig, B. (2009) The role of DNA shape in protein-DNA recognition. *Nature 461*, 1248−1253.

(7) Segal, E., Fondufe-Mittendorf, Y., Chen, L., Thastrom, A., Field, Y., Moore, I. K., Wang, J. P., and Widom, J. (2006) A genomic code for nucleosome positioning. *Nature 442*, 772−778.

(8) El Hassan, M. A., and Calladine, C. R. (1996) Propeller-twisting of base-pairs and the conformational mobility of dinucleotide steps in DNA. *J. Mol. Biol. 259*, 95−103.

(9) Packer, M. J., Dauncey, M. P., and Hunter, C. A. (2000) Sequence-dependent DNA structure: Tetranucleotide conformational maps. *J. Mol. Biol. 295*, 85−103.

(10) Gardiner, E. J., Hunter, C. A., Packer, M. J., Palmer, D. S., and Willett, P. (2003) Sequence-dependent DNA structure: A database of octamer structural parameters. *J. Mol. Biol. 332*, 1025−1035.

(11) Suzuki, M., and Yagi, N. (1995) Stereochemical basis of DNA bending by transcription factors. *Nucleic Acids Res. 23*, 2083−2091.

(12) Chen, S., Vojtechovsky, J., Parkinson, G. N., Ebright, R. H., and Berman, H. M. (2001) Indirect readout of DNA sequence at the primary-kink site in the CAP-DNA complex: DNA binding specificity based on energetics of DNA kinking. *J. Mol. Biol. 314*, 63−74.

(13) Kim, Y., Geiger, J. H., Hahn, S., and Sigler, P. B. (1993) Crystal structure of a yeast TBP/TATA-box complex. *Nature 365*, 512−520.

(14) Haran, T. E., and Mohanty, U. (2009) The unique structure of A-tracts and intrinsic DNA bending. *Q. Rev. Biophys. 42*, 41−81.

(15) MacDonald, D., Herbert, K., Zhang, X., Pologruto, T., and Lu, P. (2001) Solution structure of an A-tract DNA bend. *J. Mol. Biol. 306*, 1081−1098.

(16) Stefl, R., Wu, H., Ravindranathan, S., Sklenar, V., and Feigon, J. (2004) DNA A-tract bending in three dimensions: Solving the dA4T4 vs. dT4A4 conundrum. *Proc. Natl. Acad. Sci. U.S.A. 101*, 1177−1182.

(17) Cohanim, A. B., and Haran, T. E. (2009) The coexistence of the nucleosome positioning code with the genetic code on eukaryotic genomes. *Nucleic Acids Res. 37*, 6466−6476.

(18) Segal, E., and Widom, J. (2009) Poly(dA:dT) tracts: Major determinants of nucleosome organization. *Curr. Opin. Struct. Biol. 19*, 65−71.

(19) Hogan, M., LeGrange, J., and Austin, B. (1983) Dependence of DNA helix flexibility on base composition. *Nature 304*, 752−754.

(20) Hagerman, P. J. (1985) Sequence dependence of the curvature of DNA: A test of the phasing hypothesis. *Biochemistry 24*, 7033−7037.

(21) Nagaich, A. K., Bhattacharyya, D., Brahmachari, S. K., and Bansal, M. (1994) CA/TG sequence at the 5′ end of oligo(A)-tracts strongly modulates DNA curvature. *J. Biol. Chem. 269*, 7824−7833.

(22) Paquet, F., Gaudin, F., and Lancelot, G. (1996) Selectively ^{13}C-enriched DNA: Evidence from ^{13}C1′ relaxation rate measurements of an internal dynamics sequence effect in the lac operator. *J. Biomol. NMR 8*, 252−260.

(23) Isaacs, R. J., and Spielmann, H. P. (2001) NMR evidence for mechanical coupling of phosphate B(I)-B(II) transitions with deoxyribose conformational exchange in DNA. *J. Mol. Biol. 311*, 149−160.

(24) Okonogi, T. M., Alley, S. C., Reese, A. W., Hopkins, P. B., and Robinson, B. H. (2002) Sequence-dependent dynamics of duplex DNA: The applicability of a dinucleotide model. *Biophys. J. 83*, 3446−3459.

(25) Kojima, C., Ono, A., Kainosho, M., and James, T. L. (1998) DNA duplex dynamics: NMR relaxation studies of a decamer with uniformly ^{13}C-labeled purine nucleotides. *J. Magn. Reson. 135*, 310−333.

(26) Shajani, Z., and Varani, G. (2007) NMR studies of dynamics in RNA and DNA by ^{13}C relaxation. *Biopolymers 86*, 348−359.

(27) Shajani, Z., and Varani, G. (2008) ^{13}C relaxation studies of the DNA target sequence for HhaI methyltransferase reveal unique motional properties. *Biochemistry 47*, 7617−7625.

(28) Duchardt, E., Nilsson, L., and Schleucher, J. (2008) Cytosine ribose flexibility in DNA: A combined NMR ^{13}C spin relaxation and molecular dynamics simulation study. *Nucleic Acids Res. 36*, 4211−4219.

(29) Perez, A., Luque, F. J., and Orozco, M. (2007) Dynamics of B-DNA on the microsecond time scale. *J. Am. Chem. Soc. 129*, 14739−14745.

(30) Mura, C., and McCammon, J. A. (2008) Molecular dynamics of a κB DNA element: Base flipping via cross-strand intercalative stacking in a microsecond-scale simulation. *Nucleic Acids Res. 36*, 4941−4955.

(31) Tian, Y., Kayatta, M., Shultis, K., Gonzalez, A., Mueller, L. J., and Hatcher, M. E. (2009) ^{31}P NMR investigation of backbone dynamics in DNA binding sites. *J. Phys. Chem. B 113*, 2596−2603.

(32) Bothe, J. R., Lowenhaupt, K., and Al-Hashimi, H. M. (2011) Sequence-specific B-DNA flexibility modulates Z-DNA formation. *J. Am. Chem. Soc. 133*, 2016−2018.

(33) Nikolova, E. N., Kim, E., Wise, A. A., O'Brien, P. J., Andricioaei, I., and Al-Hashimi, H. M. (2011) Transient Hoogsteen base pairs in canonical duplex DNA. *Nature 470*, 498−502.

(34) Pèrez, A., Castellazzi, C. L., Battistini, F., Collinet, K., Flores, O., Deniz, O., Ruiz, M. L., Torrents, D., Eritja, R., Soler-Lûpez, M., and Orozco, M. (2012) Impact of Methylation on the Physical Properties of DNA. *Biophys. J. 102*, 2140−2148.
(35) Stivers, J. T. (2008) Extrahelical damaged base recognition by DNA glycosylase enzymes. *Chemistry 14*, 786−793.
(36) Patikoglou, G. A., Kim, J. L., Sun, L., Yang, S. H., Kodadek, T., and Burley, S. K. (1999) TATA element recognition by the TATA box-binding protein has been conserved throughout evolution. *Genes Dev. 13*, 3217−3230.
(37) Aishima, J., Gitti, R. K., Noah, J. E., Gan, H. H., Schlick, T., and Wolberger, C. (2002) A Hoogsteen base pair embedded in undistorted B-DNA. *Nucleic Acids Res. 30*, 5244−5252.
(38) Ughetto, G., Wang, A. H., Quigley, G. J., van der Marel, G. A., van Boom, J. H., and Rich, A. (1985) A comparison of the structure of echinomycin and triostin A complexed to a DNA fragment. *Nucleic Acids Res. 13*, 2305−2323.
(39) Ha, S. C., Lowenhaupt, K., Rich, A., Kim, Y. G., and Kim, K. K. (2005) Crystal structure of a junction between B-DNA and Z-DNA reveals two extruded bases. *Nature 437*, 1183−1186.
(40) Meints, G. A., and Drobny, G. P. (2001) Dynamic impact of methylation at the M.Hhai target site: A solid-state deuterium NMR study. *Biochemistry 40*, 12436−12443.
(41) Echodu, D., Goobes, G., Shajani, Z., Pederson, K., Meints, G., Varani, G., and Drobny, G. (2008) Furanose dynamics in the HhaI methyltransferase target DNA studied by solution and solid-state NMR relaxation. *J. Phys. Chem. B 112*, 13934−13944.
(42) Borer, P. N., LaPlante, S. R., Kumar, A., Zanatta, N., Martin, A., Hakkinen, A., and Levy, G. C. (1994) ^{13}C-NMR relaxation in three DNA oligonucleotide duplexes: Model-free analysis of internal and overall motion. *Biochemistry 33*, 2441−2450.
(43) Spielmann, H. P. (1998) Dynamics in psoralen-damaged DNA by ^{1}H-detected natural abundance ^{13}C NMR spectroscopy. *Biochemistry 37*, 5426−5438.
(44) Zimmer, D. P., and Crothers, D. M. (1995) NMR of enzymatically synthesized uniformly ^{13}C^{15}N-labeled DNA oligonucleotides. *Proc. Natl. Acad. Sci. U.S.A. 92*, 3091−3095.
(45) Hansen, A. L., and Al-Hashimi, H. M. (2007) Dynamics of large elongated RNA by NMR carbon relaxation. *J. Am. Chem. Soc. 129*, 16072−16082.
(46) Delaglio, F., Grzesiek, S., Vuister, G. W., Zhu, G., Pfeifer, J., and Bax, A. (1995) NMRPipe: A multidimensional spectral processing system based on UNIX pipes. *J. Biomol. NMR 6*, 277−293.
(47) Palmer, A. G., III, and Massi, F. (2006) Characterization of the dynamics of biomacromolecules using rotating-frame spin relaxation NMR spectroscopy. *Chem. Rev. 106*, 1700−1719.
(48) Tjandra, N., Cowburn, D., and Fushman, D. (1999) An approach to direct determination of protein dynamics from N-15 NMR relaxation at multiple fields, independent of variable N-15 chemical shift anisotropy and chemical exchange contributions. *J. Am. Chem. Soc. 121*, 8577−8582.
(49) Dethoff, E. A., Hansen, A. L., Musselman, C., Watt, E. D., Andricioaei, I., and Al-Hashimi, H. M. (2008) Characterizing complex dynamics in the transactivation response element apical loop and motional correlations with the bulge by NMR, molecular dynamics, and mutagenesis. *Biophys. J. 95*, 3906−3915.
(50) Garcia de la Torre, J., Huertas, M. L., and Carrasco, B. (2000) HYDRONMR: Prediction of NMR relaxation of globular proteins from atomic-level structures and hydrodynamic calculations. *J. Magn. Reson. 147*, 138−146.
(51) Lu, X. J., and Olson, W. K. (2008) 3DNA: A versatile, integrated software system for the analysis, rebuilding and visualization of three-dimensional nucleic-acid structures. *Nat. Protoc. 3*, 1213−1227.
(52) Case, D. A., Darden, T. A., Cheatham, T. E., III, Simmerling, C. L., Wang, J., Duke, R. E., Luo, R., Walker, R. C., Zhang, W., Merz, K. M., Roberts, B. P., Wang, B., Hayik, S., Roitberg, A., Seabra, G., Kolossváry, I., Wong, K. F., Paesani, F., Vanicek, J., Liu, J., Wu, X., Brozell, S. R., Steinbrecher, T., Gohlke, H., Cai, Q., Ye, X., Wang, J., Hsieh, M.-J., Cui, G., Roe, D. R., Mathews, D. H., Seetin, M. G., Sagui, C., Babin, V., Luchko, T., Gusarov, S., Kovalenko, A., and Kollman, P. A. (2010) *AMBER 11*, University of California, San Francisco.
(53) Humphrey, W., Dalke, A., and Schulten, K. (1996) VMD: Visual molecular dynamics. *J. Mol. Graphics 14*, 27−38.
(54) Phillips, J. C., Braun, R., Wang, W., Gumbart, J., Tajkhorshid, E., Villa, E., Chipot, C., Skeel, R. D., Kale, L., and Schulten, K. (2005) Scalable molecular dynamics with NAM. *J. Comput. Chem. 26*, 1781−1802.
(55) MacKerell, A. D., Jr., Banavali, N., and Foloppe, N. (2000) Development and current status of the CHARMM force field for nucleic acids. *Biopolymers 56*, 257−265.
(56) Barsky, D., Foloppe, N., Ahmadia, S., Wilson, D. M., III, and MacKerell, A. D., Jr. (2000) New insights into the structure of abasic DNA from molecular dynamics simulations. *Nucleic Acids Res. 28*, 2613−2626.
(57) Szabo, A., and Lipari, G. (1982) Model-free approach to the interpretation of nuclear magnetic-resonance relaxation in macromolecules. 1. Theory and range of validity. *J. Am. Chem. Soc. 104*, 4546−4559.
(58) Musselman, C., Zhang, Q., Al-Hashimi, H., and Andricioaei, I. (2010) Referencing Strategy for the Direct Comparison of Nuclear Magnetic Resonance and Molecular Dynamics Motional Parameters in RNA. *J. Phys. Chem. B 114*, 929−939.
(59) Clore, G. M., Szabo, A., Bax, A., Kay, L. E., Driscoll, P. C., and Gronenborn, A. M. (1990) Deviation from the simple 2-parameter model-free approach to the interpretation of N-15 nuclear magnetic-relaxation of proteins. *J. Am. Chem. Soc. 112*, 4989−4991.
(60) Henry, E. R., and Szabo, A. (1985) Influence of vibrational motion on solid-state line-shapes and NMR relaxation. *J. Chem. Phys. 82*, 4753−4761.
(61) Brooks, B. R., Bruccoleri, R. E., Olafson, B. D., States, D. J., Swaminathan, S., and Karplus, M. (1983) CHARMM: A program for macromolecular energy, minimization, and dynamics calculations. *J. Comput. Chem. 4*, 187−217.
(62) Allen, M. P., and Tildesley, D. J. (1987) *Computer simulation of liquids*, Oxford University Press, Inc., New York.
(63) Marini, J. C., Levene, S. D., Crothers, D. M., and Englund, P. T. (1982) Bent helical structure in kinetoplast DNA. *Proc. Natl. Acad. Sci. U.S.A. 79*, 7664−7668.
(64) Kintanar, A., Klevit, R. E., and Reid, B. R. (1987) Two-dimensional NMR investigation of a bent DNA fragment: Assignment of the proton resonances and preliminary structure analysis. *Nucleic Acids Res. 15*, 5845−5862.
(65) Katahira, M., Sugeta, H., Kyogoku, Y., Fujii, S., Fujisawa, R., and Tomita, K. (1988) One- and two-dimensional NMR studies on the conformation of DNA containing the oligo(dA)oligo(dT) tract. *Nucleic Acids Res. 16*, 8619−8632.
(66) Zhang, Q., Sun, X., Watt, E. D., and Al-Hashimi, H. M. (2006) Resolving the motional modes that code for RNA adaptation. *Science 311*, 653−656.
(67) Nikolova, E. N., and Al-Hashimi, H. M. (2009) Preparation, resonance assignment, and preliminary dynamics characterization of residue specific ^{13}C/^{15}N-labeled elongated DNA for the study of sequence-directed dynamics by NMR. *J. Biomol. NMR 45*, 9−16.
(68) Duchardt, E., and Schwalbe, H. (2005) Residue specific ribose and nucleobase dynamics of the cUUCGg RNA tetraloop motif by MNMR ^{13}C relaxation. *J. Biomol. NMR 32*, 295−308.
(69) Shajani, Z., and Varani, G. (2005) ^{13}C NMR relaxation studies of RNA base and ribose nuclei reveal a complex pattern of motions in the RNA binding site for human U1A protein. *J. Mol. Biol. 349*, 699−715.
(70) Leroy, J. L., Charretier, E., Kochoyan, M., and Gueron, M. (1988) Evidence from base-pair kinetics for two types of adenine tract structures in solution: Their relation to DNA curvature. *Biochemistry 27*, 8894−8898.
(71) Isaacs, R. J., and Spielmann, H. P. (2004) Insight into G−T mismatch recognition using molecular dynamics with time-averaged restraints derived from NMR spectroscopy. *J. Am. Chem. Soc. 126*, 583−590.

(72) Chen, J., Dupradeau, F. Y., Case, D. A., Turner, C. J., and Stubbe, J. (2008) DNA oligonucleotides with A, T, G or C opposite an abasic site: Structure and dynamics. *Nucleic Acids Res. 36*, 253−262.
(73) LaPlante, S. R., Zanatta, N., Hakkinen, A., Wang, A. H., and Borer, P. N. (1994) ^{13}C-NMR of the deoxyribose sugars in four DNA oligonucleotide duplexes: Assignment and structural features. *Biochemistry 33*, 2430−2440.
(74) Foloppe, N., and MacKerell, A. D., Jr. (1999) Intrinsic conformational properties of deoxyribonucleosides: Implicated role for cytosine in the equilibrium among the A, B, and Z forms of DNA. *Biophys. J. 76*, 3206−3218.
(75) Lefebvre, A., Mauffret, O., Lescot, E., Hartmann, B., and Fermandjian, S. (1996) Solution structure of the CpG containing d(CTTCGAAG)$_2$ oligonucleotide: NMR data and energy calculations are compatible with a BI/BII equilibrium at CpG. *Biochemistry 35*, 12560−12569.
(76) Madhumalar, A., and Bansal, M. (2005) Sequence preference for BI/BII conformations in DNA: MD and crystal structure data analysis. *J. Biomol. Struct. Dyn. 23*, 13−27.
(77) Heddi, B., Foloppe, N., Bouchemal, N., Hantz, E., and Hartmann, B. (2006) Quantification of DNA BI/BII backbone states in solution. Implications for DNA overall structure and recognition. *J. Am. Chem. Soc. 128*, 9170−9177.
(78) Rauch, C., Trieb, M., Wellenzohn, B., Loferer, M., Voegele, A., Wibowo, F. R., and Liedl, K. R. (2003) C5-methylation of cytosine in B-DNA thermodynamically and kinetically stabilizes BI. *J. Am. Chem. Soc. 125*, 14990−14991.
(79) Parkinson, G., Wilson, C., Gunasekera, A., Ebright, Y. W., Ebright, R. E., and Berman, H. M. (1996) Structure of the CAP-DNA complex at 2.5 angstroms resolution: A complete picture of the protein-DNA interface. *J. Mol. Biol. 260*, 395−408.
(80) Kitayner, M., Rozenberg, H., Rohs, R., Suad, O., Rabinovich, D., Honig, B., and Shakked, Z. (2010) Diversity in DNA recognition by p53 revealed by crystal structures with Hoogsteen base pairs. *Nat. Struct. Mol. Biol. 17*, 423−429.